

<https://doi.org/10.1038/s42005-025-02007-2>

# On-fiber photonic nanojet enables super-resolution in en face optical coherence tomography and scattering nanoscopy

Kaushal Vairagi<sup>1</sup>, Jasleen Kaur<sup>1,2</sup>, Pooja Gupta<sup>1</sup>, Stefan Enoch<sup>3</sup> & Samir K. Mondal<sup>1</sup>✉

Photonic nanojet (PNJ) of subwavelength spot-size originating at shadow side of a microsphere is projected as an imperative optical tool for micro-nano optics applications. Lack of a free hold PNJ source limits its vast potential. A state-of-the-art PNJ is introduced on a chemically etched encaved optical fiber nanoprobe holding a microsphere. Nanoprobe generating optical beam of spot-size  $\sim 2 \mu\text{m}$ , is focused on the microsphere resulting in PNJ of varying spot-size,  $0.8\lambda$  to  $0.5\lambda$ , over its' length  $\sim 13\lambda$  at 660 nm wavelength. A PNJ centered around 840 nm wavelength combined with an effective numerical aperture  $\sim 2$  results in an en-face optical coherence tomography (OCT) image of lateral resolution  $\sim 247 \text{ nm}$  and phase map with optical thickness,  $\sim 70 \text{ nm}$  for a standard DVD. Further, the PNJ based backscattered nanoscopy of silver nano-particles is exhibited with resolution  $\sim 40 \text{ nm}$ . This commercially viable PNJ head can be an ideal platform for various microscopies and other applications.

The pursuit of sub-diffraction confinement of light and power concentration has been a longstanding focus of research, dating back to the early predictions of optical resolution and the diffraction limit. It is still a challenge as the application of optics, especially in nano-domain, is experiencing a significant progress even beyond optical imaging. In this context, the optical confinement of an instrument in the far-field is guided by Abbe-Rayleigh's criteria. According to the criteria, the resolution of an optical sensing instrument is limited by the spot-size of the optical beam, analogous to uncertainty principle in quantum mechanics<sup>1–3</sup>. It is incapable of resolving higher frequencies responsible for the object sharpness because of the diffraction limit. Consequently, the wave optics restricts this limit to  $\lambda/(2\text{NA})^1$  for an objective lens, where NA stands for numerical aperture of the lens and  $\lambda$  represents the illuminating wavelength. A more practical approach to this resolution limit is defined in terms of full width at half maximum (FWHM) or spot-size,  $\omega = (0.51\lambda)/\text{NA}$ , which is approximately equal to Abbe's definition. FWHM serves as a key parameter for evaluating the optical confinement and optical resolution because it is relatively easy to measure and widely accepted. The ability to visualize objects in nano-scale through imaging or spectroscopy relies on the optical beam's spot-size being compressed beyond the classical diffraction limit.

Alternately, the near-field approach offers an intriguing perspective by utilizing non-propagating evanescent waves to surpass the diffraction limit. However, the non-propagating evanescent waves, characterized by  $\sim e^{-kz}$ , contain subwavelength information but they are confined solely to the

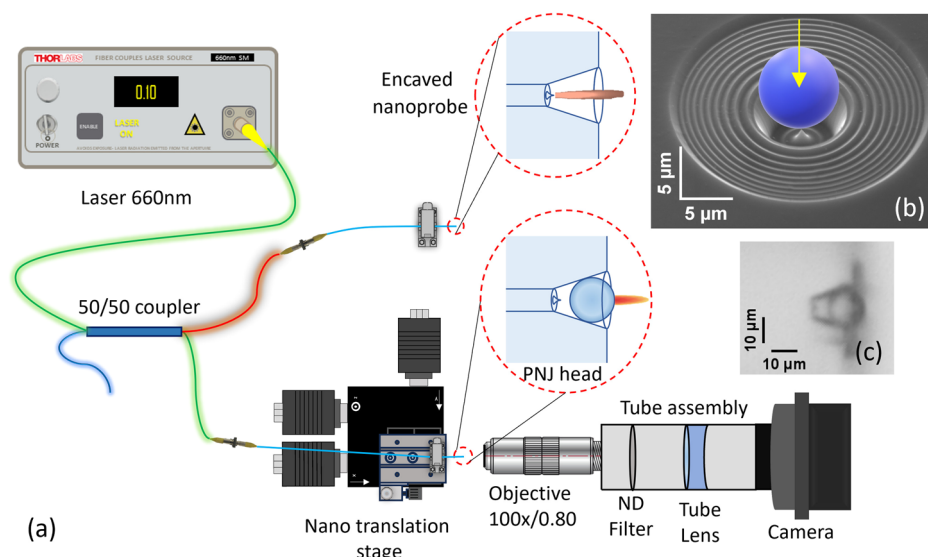
surface<sup>4</sup>. Thus, probing the evanescent wave is quite difficult due to its rapid decay unlike far-field diffraction, demanding complex mechanical and optical arrangements. Moreover, it is limited by practically zero working distance and an extremely small depth of field. Despite these challenges, the last decades have seen several breakthroughs in imaging techniques that have gone beyond the diffraction limit<sup>5–9</sup>. Therefore, a simple far-field optics approach with sub diffraction confinement can be highly valuable for photonics application and a photonic nanojet (PNJ)<sup>10</sup> with subwavelength spot-size is found to be an ideal tool in this regard.

The phenomenon of PNJ is a non-resonant and non-evanescent by nature. It can be explained by Mie's theory of scattering, which predicts the field enhancement by microspheres transforming from the Rayleigh scattering regime ( $r \ll \lambda$ ) to a jet-like regime in mesoscale spheres ( $r \sim \lambda - 30\lambda$ )<sup>11,12</sup>. Depending on the excitation conditions, it can either confine the light inside the cavity, forming WGMs or focus the light in proximity to the shadow side, resulting in the formation of PNJ. The localized PNJ forms along the line of incidence at the shadow-side surface of the microsphere and exhibits the non-diffracting characteristics of light over a distance of several wavelengths with a sub-wavelength spot-size<sup>13,14</sup>. This can be possible due to the interference between incident light and scattered light.

Since its introduction, PNJ has provided an immense impact on super-resolution optical imaging<sup>10,15,16</sup> fluorescence spectroscopy<sup>17</sup>, enhancement of Raman scattering<sup>18,19</sup>, nanoparticles sensing<sup>20–22</sup>, nanolithography<sup>23,24</sup>, and many others<sup>25</sup> due to the backscattering enhancement<sup>26</sup> and sub-diffraction

<sup>1</sup>CSIR- Central Scientific Instruments Organisation, Chandigarh, India. <sup>2</sup>Academy of Scientific & Innovative Research, Ghaziabad, UP, India. <sup>3</sup>Aix Marseille Univ, CNRS, Centrale Marseille, Institut Fresnel, Marseille, France. ✉e-mail: [samir\\_mondal@csio.res.in](mailto:samir_mondal@csio.res.in)

**Fig. 1 | Schematic of the experimental set up for capturing the beam profile in air from the Photonic nanojet (PNJ) head with the microsphere and the nanoprobe. a** The 660 nm laser source is coupled to a 50/50 coupler whose one output arm (orange branch) holds the nanoprobe while another (green branch with Nano translation) holds the PNJ head. The coupler assures the same power goes to both the arms while profiling the respective beam using custom made near field beam profiler consisting of an objective, tube assembly and CMOS camera. **b** shows a Field Emission Scanning Electron Microscopy (FESEM) image of the nanoprobe to demonstrate that how a microsphere is placed inside the cavity of the nanoprobe and (c) shows an optical microscopic image of PNJ head.



field confinement. The further development and application of photonic nanojets could provide useful new approaches for conducting inverse-scattering studies of weakly contrasting micron-scale material objects. As of now, the microsphere needs to be held by a cantilever<sup>27</sup>/capillary<sup>28</sup>/optical tweezer<sup>29</sup>/PDMS film<sup>30</sup> and the illumination is provided by the microscopic objective for line-of-sight imaging majorly in contact mode. While for the sensing applications optical fiber based excitation of photonic nanojets has been reported by temporary tweezing<sup>21,22</sup>, the imaging aspect of this simple approach using low coherence interferometry is still untouched despite of the fact that it can provide the lateral resolution improvement upto one third of the spot size<sup>31</sup>. To access the full potential of this approach in sensing as well as imaging there is a need of a standalone PNJ head especially if it can be designed at an optical fiber tip. The ability of PNJs to move freely can open the numerous horizons of application assisted with the waveguide nature of the optical fiber.

In this letter, a standalone PNJ head is developed at the tip of an optical fiber. It consists of a nanoprobe located within the cavity of an optical fiber tip fabricated using a one-step chemical etching process. The nanoprobe generates a focused optical beam with a tight spot-size of  $\sim 2 \mu\text{m}$ . The cavity in front of the nanoprobe holds a microsphere, and thus the optical beam from the nanoprobe can be focused on the microsphere, resulting in a quality PNJ. The proposed PNJ head is free to move and suitable for use in both reflection and transmission mode. As an application of this standalone PNJ head, we have demonstrated an OCT resulting in a super resolution en face image beyond the spot-size ( $\omega$ ) restricted diffraction limit,  $< \omega$ , as well as sub diffraction scattered light field imaging of nano-particles as revealed in the sections below.

## Methods

### Materials

The Barium titanate microspheres of diameter  $5 \mu\text{m}$ – $50 \mu\text{m}$  were brought from sigma-aldrich, 48% hydrofluoric (HF) acid from Merck and the GF3 optical fiber from Coherent.

### Nanoprobe fabrication

The encaved nanoprobe is fabricated through chemical etching of a highly germanium doped optical fiber (GF3) using 48% HF. Initially, the optical fiber is stripped, cleaned and cleaved before being vertically immersed in HF acid contained within a plastic tube, with a protective layer of toluene placed above the HF. The higher doping concentration in the core results in a faster etching rate compared to the cladding, leading to upward etching from the facet of the optical fiber. This upward etching forms a conical cavity along the core-cladding boundary with the apex located at the core, and a conical

tip in the core at the center of the apex due its refractive index profile. The formation of conical tip in the core can be explained by the fact that there is a defect due to non-uniform material distribution at the center of the core of the optical fiber along the optical axis. The circular defect has diameter  $\sim 2 \mu\text{m}$  as observed from the optical microscopic image of the fiber tip, as shown in the Supplementary Fig. 1. This results in mismatch in etching rate of the optical fiber materials at the fiber cladding, core and the very center of the core in HF solution. The part of the core surrounding the defect zone has higher etching rate due to higher Ge concentration compared to the cladding and the center of the core. The said mismatch develops a conical nanoprobe around the optical axis with base diameter  $< 2 \mu\text{m}$  and height  $\sim 1 \mu\text{m}$  at the center surrounded by the cavity as soon as one dips the optical fiber in HF solution<sup>32</sup>. The conical nanoprobe is recreated dynamically and the shape remains constant as long as etching continues except varying the length of the cavity. The technique is introduced recently to develop encaved nanoprobe at optical fiber tip<sup>33</sup>. The cavity length can be precisely controlled by etching time, while the conical tip structure remains unaltered. Upon reaching the desired etching time, the optical fiber is removed from the HF and rinsed in a stream of deionized (DI) water followed by annealing to evaporate any trapped water from the cavity. In our experiments, we have used the PNJ probe with a 3 min etching time, resulting in a cavity length of  $\sim 17 \mu\text{m}$  and opening diameter of  $\sim 19 \mu\text{m}$ . The nanoprobe is fabricated inside the optical fiber tip as observed in Fig. 1b (field emission scanning electron microscope (FESEM) image of the cavity). The recent development of the optical fiber nanoprobe is a well-known fact for its maturity, interesting optics and application<sup>33–37</sup>.

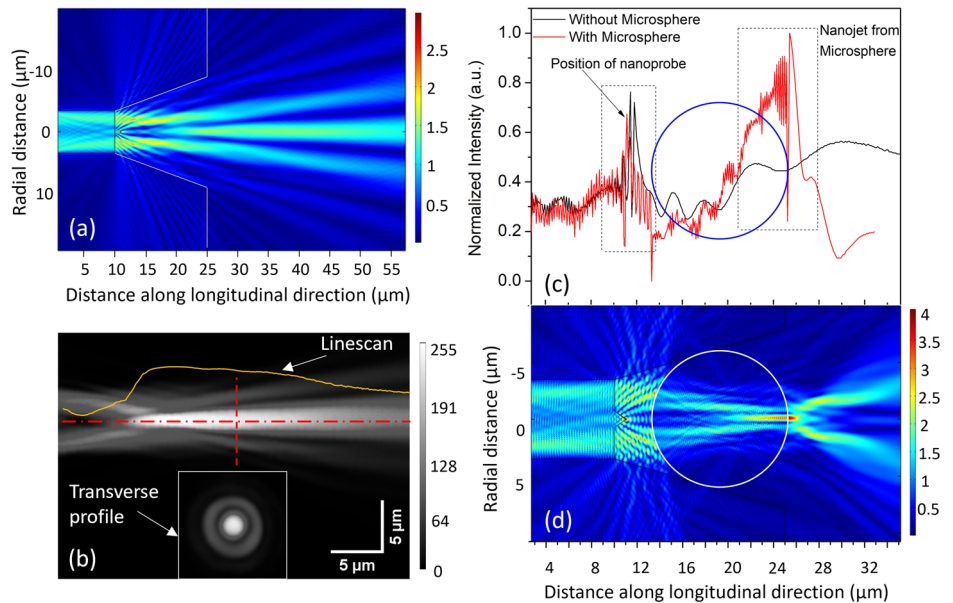
### Microsphere integration

The microspheres are scattered onto a glass slide under a calibrated stereo microscope equipped with a camera. A microsphere of the desired diameter is then selected and picked up electrostatically on the tip of a tapered optical fiber mounted on a 5 axis-manual translation stage. Subsequently, the optical fiber carrying the microsphere is aligned with the encaved nanoprobe which is mounted on another 5-axis manual translation stage. Finally, the microsphere is meticulously positioned and pushed inside the cavity, and then we drag out the tapered tip fiber sideways leaving the particle in the cavity. A pictorial representation is shown in Fig. 1b to elaborate how a microsphere is placed inside the cavity of the nanoprobe. Additionally, an optical microscopic image of a standalone PNJ head is showcased in Fig. 1c.

### Beam profiling

For PNJ beam profiling we have used a home-made near field beam profiler comprising a  $100\times/0.8$  NA infinity corrected apochromatic objective lens

**Fig. 2 | PNJ head design optimization.** **a** COMSOL simulation of the optics from nanoprobe inside the optical fiber tip cavity. **b** Experimentally obtained beam profile from a nanoprobe in a longitudinal plane through the beam axis, the linescan along the central axis (horizontal red line) indicates variation in intensity with propagation, the inset is the transverse beam profile taken across the vertical red dashed line. It shares the same scale of figure (b) itself. **c** Represents an intensity comparison of the simulation results between the nanoprobe beam and PNJ, longitudinally along the optical axis. The blue circle shows the position and outline of microsphere. **d** COMSOL simulation of the PNJ from the microsphere placed at the opening of the cavity in front of the nanoprobe. Both the figure (c, d) are concatenated and shares the same X axis. This helps to understand how the field varies relative to the position of nanoprobe and microsphere.



integrated into a tube assembly along with a neutral density (ND) filter, a 200 mm tube lens and a 20MP CMOS camera. Figure 1a depicts the schematic of the experimental setup to capture the PNJ as well as the nanoprobe beam profiles in air. The setup is calibrated with a USAF 1951 resolution target. A 660 nm fiberized benchtop laser from Thorlabs is employed as a source for this experiment. The light is guided through a 670 nm, single mode fused optical fiber 50–50 coupler to two output arms: an encaved nanoprobe (S1) and a PNJ probe (S2). The beam profiling of both the sample probes S1 & S2 is carried out one by one at the same input power for intensity enhancement comparison.

The sample is mounted on a tilt stage which in turn is fixed on 3-axis nanoMAX from Thorlabs. Throughout the experiment, the beam profiler is kept stationary while the sample undergoes translational motion. Initially, the beam profiler is focused on the facet of the nanoprobe to mark the reference position. Consequently, the focus is then shifted inside the cavity upto the measured cavity length to begin the profiling. The focus is then translated in the direction of beam propagation with the step size of 60 nm and an image is captured at each step over a total length of 22 μm. Furthermore, these images are stacked to construct a 3D beam profile using Fiji<sup>38</sup> and a plane along the direction of propagation is extracted to show 2D beam profile in longitudinal direction.

As the nanojet is ready, the PNJ head is used as a probe to scan a DVD surface to examine performance of the nanojet as an interferometric en face OCT probe with sub-diffraction resolution including phase imaging. Further, the probe is tested for scattering nanoscopy by scanning silver nanoparticles on a glass slide.

### Enface OCT imaging and phase imaging processing

We have used the similar setup as briefly described in our earlier work<sup>39</sup>, with the only difference in the sample placement, the imaging sample is now mounted vertically, while the PNJ probe is kept horizontal (Supplementary Fig. 2). A standard Fourier transform algorithm is used for en face OCT imaging. For phase imaging, a Fourier transform based phase retrieval algorithm is applied in spectral-domain<sup>40</sup>. The desired phase,  $\phi(z)$  in terms of optical path length,  $\Delta L(z)$  as a function of depth,  $z$  is estimated using Eq. (1).

$$\phi(z)|_{(x,y)} = \frac{4\pi}{\lambda_0} \Delta L(z) \quad (1)$$

## Results & Discussion

### PNJ simulation results

The simulations are performed using COMSOL to evaluate the background of the prospective PNJ before conducting experimental investigation. Figure 2a, b shows the simulated and experimental beam profile respectively in a longitudinal plane through the optical axis radiating from the nanoprobe. The nanoprobe generates zeroth order Bessel-Gauss beam characterized with a prominent central lobe having spot-size of  $\sim 2 \mu\text{m}$  at  $\sim 14 \mu\text{m}$  distance from the probe tip.

For PNJ generation, a microsphere of diameter  $12 \mu\text{m}$  is strategically placed at  $\sim 3 \mu\text{m}$  from the probe tip. The diameter and location of the microsphere are selected to ensure that the central spot of the Bessel-Gauss beam having higher intensity converges at the vicinity of the distal end of the microsphere, as presented in Fig. 2d, a prerequisite condition for PNJ generation<sup>11</sup>.

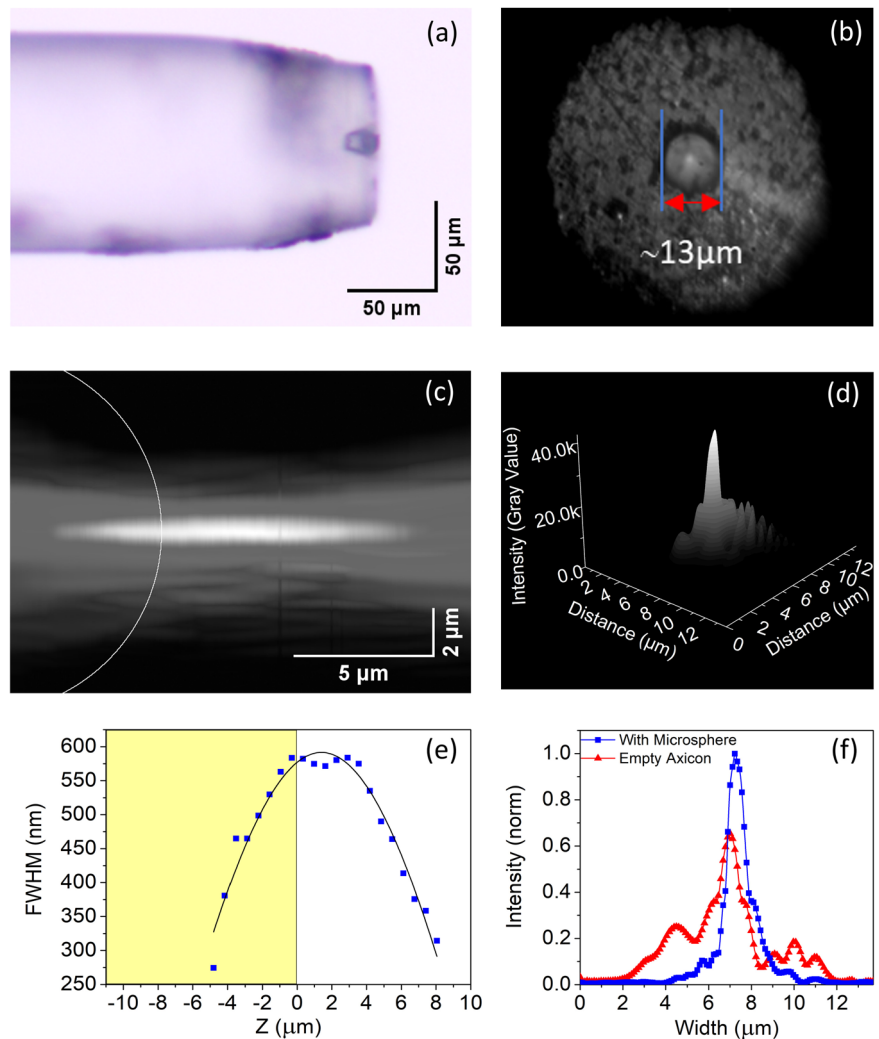
The simulation is performed for the wavelength,  $\lambda = 660 \text{ nm}$  and the spot-size of the simulated PNJ is obtained as  $\sim 0.5\lambda$ . Subsequently, the intensity of the PNJ formed at the shadow side of the microsphere is compared in Fig. 2c with the intensity of the beam generated solely by the nanoprobe. It is observed that the intensity of the PNJ experiences  $\sim 1.75$  times increase in the field intensity in comparison to the nanoprobe beam.

### Characterization of the PNJ

Figure 3 demonstrates a comprehensive overview of the experimental results related to the PNJ. Figure 3a, b, present side view and front view of the PNJ head respectively. Figure 3c, d showcase the beam characteristics of the PNJ captured by a homemade beam profiler with  $100\times/0.80$  dry microscopic objective. The profiler setup is configured for a 660 nm source coupled to the nanoprobe fiber as schematically shown in Fig. 1a. The 3D beam profile of the PNJ at the plane of the highest intensity is represented in Fig. 3d. However, the evolution of the PNJ along its length is illustrated in 3D animation (Supplementary Movie). The nanojet originates inside the microsphere and extends to  $\sim 8 \mu\text{m}$ , ( $13\lambda$ ) beyond the microsphere surface.

Figure 3e depicts the variation of the spot-size ( $\omega$ ) of the PNJ across its entire length, ranging from a maximum,  $\omega \sim 550 \text{ nm}$  ( $0.8\lambda$ ) to a minimum,  $\omega \sim 300 \text{ nm}$  ( $0.5\lambda$ ). The experimentally attained minimum spot-size,  $\sim 0.5\lambda$  matches with the spot-size obtained in the PNJ simulated results. The colored half of Fig. 3e corresponds to the region within the microsphere,

**Fig. 3 | Characterization of PNJ head.** **a** Top view optical microscopic image of cavity with nanoprobe holding a microsphere,  $\sim 13 \mu\text{m}$  diameter as PNJ head. **b** Front view of the microsphere placed at the cavity opening and near to the nanoprobe. **c** Beam profiling of photonic nanojet from the microsphere, the white curve indicates microsphere's boundary. **d** 3D beam-profile of the nano-jet taken at a selective transverse plane with highest intensity in the PNJ from (c). **e** Variation in the spot-size,  $\omega$  over the length of the PNJ. The yellow shaded area lies inside the microsphere. **f** Transverse beam profiles of the beam from nanoprobe (red triangles) and PNJ (blue solid square) at the plane of the highest intensity.



while the remaining part represents the region outside the microsphere. This visualization is generated by tracing the beam as the beam profiler initially focuses inside the microsphere, while the PNJ head placed on nano-stage is slowly moved away by 60 nm step-size. The transverse beam profiles of the PNJ and nanoprobe at the plane of maximum intensity are compared, as illustrated in Fig. 3f. It is evident from the experimental results that the PNJ experiences  $\sim 1.5$ -fold increase in the intensity, which is in accordance to the simulation result. However, a focal shift in the PNJ can be observed between the simulation and experimental result whereas the length of the PNJ closely matches. The mismatch in 2D simulation and 3D experimental results may be due to approximation in the material property of the microsphere and geometry of nanoantenna used in the simulation, including non-ideal geometry of the microsphere used in the experiment in terms of non-sphericity. Moreover, the PNJ exhibits a tighter spot-size and more importantly, it is free from any significant sidelobes.

### En face Optical Coherence Tomography (OCT) and Phase imaging

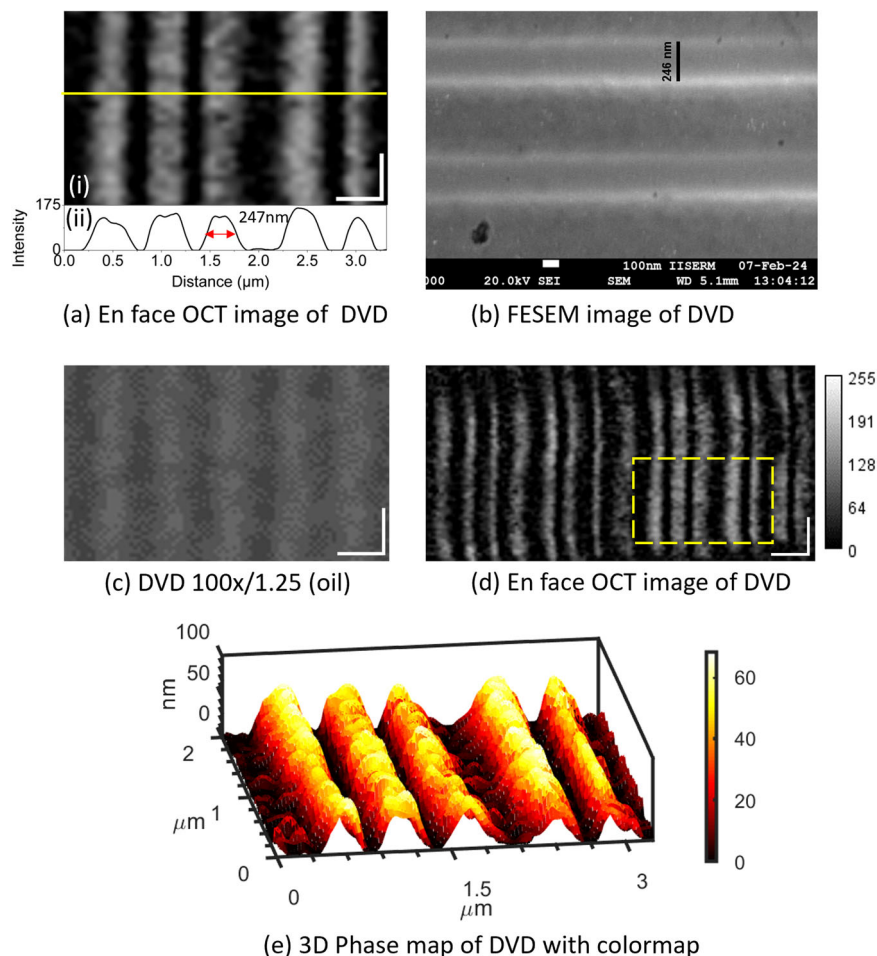
As an application of the state-of-the-art tool, an imaging experiment is performed for super-resolution en face OCT imaging including phase imaging and results are discussed in the following section. A common-path OCT experimental arrangement has been employed for the imaging (Supplementary Fig. 2). For the PNJ beam profiling, a 660 nm monochromatic laser source is used whereas en face OCT requires broad band source. Accordingly, a source with bandwidth  $\sim 50$  nm centered at 840 nm, usually recommended for OCT, is used for the nanoscopy imaging.

A highly reflective DVD as a sample, positioned vertically from 3 μm to 4 μm away on a translational nano-stage in front of the PNJ head. The sample is then scanned over an area of  $10 \mu\text{m} \times 5 \mu\text{m}$  in the transverse plane with a step size of 60 nm for each scan. The optical fiber tip is placed in the V-groove in an optical fiber holder to assure its alignment. Also, the working distance between the microsphere and the sample is several micrometers unlike many scanning devices with nanometer working distance. Therefore, small misalignment may not be an issue unless we scan a very big area in one go. En face image of the DVD sample from the common-path OCT system with SNR  $\sim 42$  dB is displayed in Fig. 4d. Whereas, Fig. 4a, e present the en face and phase image of the DVD with an area of  $3 \mu\text{m} \times 2 \mu\text{m}$  which is the region marked by yellow rectangular box in Fig. 4d. Figure 4c is the microscopic image of the DVD taken under  $100\times$  objective with numerical aperture 1.25 in oil which is in close match to the Fig. 4a obtained from the proposed system. A line scan along the yellow line from the en face OCT image is concatenated with the image sharing the same horizontal scale in Fig. 4a. The line scan reveals that the proposed OCT system can achieve sub-diffraction resolution,  $\sim 247$  nm. The resolution is also confirmed by the supporting FESEM image of the same DVD sample, as shown in Fig. 4b. Further, the 3D phase image of the DVD provides an optical thickness of  $\sim 70$  nm as indicated by the colorbar in Fig. 4e.

The imaging resolution provided by PNJ in air is equivalent to the standard optical microscopic system having numerical aperture of 2.07 (Rayleigh criteria) and 1.7 (Abbe's criteria). Notably, the obtained resolution is comparable to the standard fluorescence system, such as a confocal microscope, where the lateral resolution is limited to around 200 to



**Fig. 4 | En face OCT as a proof of the PNJ's capability to image beyond the diffraction limit and to scan the sample as well.** **a** An en face OCT image of DVD: (i) The DVD grating shows a resolution  $\sim 246$  nm,  $\sim 0.3$  times the wavelength used in the experiment, the dimension of scale bar is 500 nm. The concatenated graph (ii) shows a linescan of the OCT image at position marked by yellow line. **b** FESEM image of the said DVD with gold coating predicts a resolution  $\sim 246$  nm confirming the OCT resolution. **c**  $100\times$  microscopic image of the DVD sample taken with 1.25 NA objective in oil, the dimension of scale bar is 500 nm. **d** A larger area En face OCT image of the DVD, yellow box highlights panel (a(i)), the scalebar is  $1\ \mu\text{m}$ . **e** 3D phase image of the DVD sample with a colorbar representing the optical thickness,  $\sim 70$  nm.



250 nm<sup>41</sup>. Additionally, there is a possibility of achieving even better resolution as evidenced by the experimental results yielding fully resolved image with a resolution of 247 nm.

The en face provides the efficient surface analysis with high resolution and depth profile. The finest spatial resolution achieved by en face OCT is  $\sim 0.7\ \mu\text{m}$  in time domain<sup>42</sup>. Scholler et al. has showcased a multimodal OCT having  $\sim 1.7\ \mu\text{m}$  and  $\sim 0.4\ \mu\text{m}$ , i.e.,  $2.02\lambda$  and  $0.6\lambda$  lateral resolution at 840 nm and 660 nm wavelength, respectively<sup>43</sup>. The en face OCT system usually achieves lateral resolutions down to  $\sim 1\text{--}2\ \mu\text{m}$ <sup>44–47</sup>. However, by providing a resolution of  $0.24\ \mu\text{m}$  i.e.,  $0.29\lambda$  the proposed system outperforms the existing literature in terms of lateral resolution.

### PNJ Scattering Nanoscopy

PNJ is highly effective in enhancing back-scattering when a nano object enters the nanojet which could be beneficial for fluorescence and Raman spectroscopy applications without surface modification. The enhancement factor of the proposed PNJ has been tested using a single grating of the DVD as scatterer. The PNJ head is scanned across and away from the grating using the similar experimental arrangement. Figure 5a plots the back-scattered field as a function of longitudinal distance. It is observed that the back scattered field for  $\sim 250$  nm scatterer placed within  $4\ \mu\text{m}$  to  $5\ \mu\text{m}$  from the microsphere is enhanced by  $\sim 10$  fold due to the nanojet. Beyond the nanojet, the scattered field sharply drops. A second, but weaker enhancement peak is observed, which may be due to the intense light at the focal length ( $\sim 8\ \mu\text{m}$ ) of the microsphere acting as a ball lens. Although beam profiling is not repeated for 840 nm source, the  $\sim 10$  times back scattering enhancement, Fig. 5a, indicates that the design also gives PNJ at 840 nm wavelength which is further confirmed by the simulation result, (Supplementary Fig. 3). The

same source is again used for silver nano-rods characterization in reflection mode due to the already available experimental setup.

To assess the PNJ head's capacity to capture scattering light from a scatterer, we have done point by point intensity mapping of the DVD nanostructure and silver nano-particles (35 nm–150 nm) drop-casted on a glass slide using the same experimental setup as in case of enface OCT imaging. The intensity value is obtained by integrating the spectrum recorded at a point. Figure 5a-inset shows the intensity mapped image of DVD where the grating structure can be seen. The result presented in Fig. 5b show that the PNJ can detect silver nano-particles, as small as  $\sim 40$  nm by mapping the intensity of the back-scattered field from the particles. This suffice the fact that the PNJ may also be suitable for Raman, and fluorescence spectroscopy.

Further, it may be mentioned that the length of photonic nanojet can be improved by truncating the microsphere (Supplementary Fig. 5). In the long term, the PNJ head holds great promise for optical imaging, nanolithography, optical trapping etc. and also generating complex photonic hook<sup>48</sup> (Supplementary Fig. 6).

### Conclusion

In summary, we have introduced a state-of-the-art standalone photonic nanojet head at optical fiber tip capable of generating long range,  $\sim 13\lambda$ , nanojet with subwavelength spot-size,  $0.5\lambda$ . It can be useful in remote sensing application, demanding sub-diffraction resolution. As a proof, optical coherence en face and phase imaging are performed on standard DVD. The experimental results show the sub-diffraction spatial resolution of  $\sim 247$  nm ( $0.29\lambda$ ) with a 42 dB SNR and  $\sim 70$  nm optical thickness for  $\sim 840$  nm illumination. Our imaging system offers the resolution equivalent

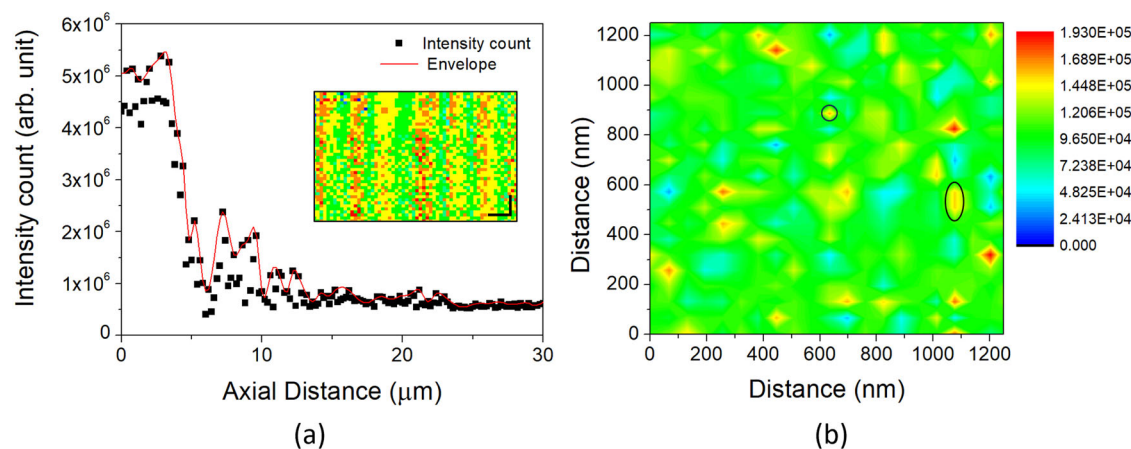


**Fig. 5 | Backscattering enhancement of PNJ and nanoscopy experimentation.** **a** Enhancement of the PNJ optical field as the probe is gradually scanned away from DVD line grating as the scatterer. Inset is the scattered field intensity mapped image of the grating lines, scale bar indicated 500 nm. **b** Intensity mapping of the back

scattering of silver nano-particle samples, drop casted on a glass slide, ranging from 35 nm to 150 nm, using the same PNJ head. Supplementary Fig. 4 shows a SEM image of the silver nanoparticles resembling the scattering results (**b**). The sample is prepared by drop casting of diluted silver nano-particle solution.

to a numerical aperture of 2.074 in a standard optical microscopic system. Additionally, the intensity mapping of silver nano-particle as light scatterer with an achieved detection capacity of ~40 nm suggests the PNJ head will also be ideal for high-resolution fluorescence, and light-scattering microscopy application. Another significant advantage is the repeatability and reproducibility of the PNJ head, as the natural chemical process ensures the cavity and the nanoprobe fabrication as long as a proper optical fiber is chosen.

### Data availability

The data supporting the findings of this study are available from the corresponding author upon reasonable request.

Received: 15 October 2024; Accepted: 14 February 2025;

Published online: 05 March 2025

### References

- Rayleigh, Lord XXXI. Investigations in optics, with special reference to the spectroscope. *Lond. Edinb. Dublin Philos. Mag. J. Sci.* **8**, 261–274 (1879).
- Born, M. & Wolf, E. *Principles of Optics*. Cambridge university press (2002).
- Stelzer, E. H. K. & Grill, S. Uncertainty principle applied to estimate focal spot dimensions. *Opt. Commun.* **173**, 51–56 (2000).
- van Hulst, N. F., De Boer, N. P. & Bölger, B. An evanescent-field optical microscope. *J. Microsc.* **163**, 117–130 (1991).
- Park, S. et al. Label-free adaptive optics single-molecule localization microscopy for whole zebrafish. *Nat. Commun.* **14**, 4185 (2023).
- Gould, T. J., Burke, D., Bewersdorf, J. & Booth, M. J. Adaptive optics enables 3D STED microscopy in aberrating specimens. *Opt. Express* **20**, 20998–21009 (2012).
- Urban, N. T., Willig, K. I., Hell, S. W. & Nägerl, U. V. STED nanoscopy of actin dynamics in synapses deep inside living brain slices. *Biophys. J.* **101**, 1277–1284 (2011).
- Zheng, W. et al. Adaptive optics improves multiphoton super-resolution imaging. *Nat. Methods* **14**, 869–872 (2017).
- Burke, D., Patton, B., Huang, F., Bewersdorf, J. & Booth, M. J. Adaptive optics correction of specimen-induced aberrations in single-molecule switching microscopy. *Optica* **2**, 177 (2015).
- Chen, Z., Taflove, A. & Backman, V. Photonic nanojet enhancement of backscattering of light by nanoparticles: a potential novel visible-light ultramicroscopy technique. *Opt. Express* **12**, 1214 (2004).
- Darafsheh, A. Photonic nanojets and their applications. *J. Phys. Photonics* **3**, 022001 (2021).
- Luk'yanchuk, B. S., Paniagua-Domínguez, R., Minin, I., Minin, O. & Wang, Z. Refractive index less than two: photonic nanojets yesterday, today and tomorrow. *Opt. Mater. Express* **7**, 1820 (2017).
- Pianta, M. et al. Direct imaging of photonic nanojets. *Opt. Express* **16**, 6930–6940 (2008).
- Bon, P. et al. Imaging the Gouy phase shift in photonic jets with a wavefront sensor. *Opt. Lett.* **37**, 3531 (2012).
- Wang, Z. et al. Optical virtual imaging at 50 nm lateral resolution with a white-light nanoscope. *Nat. Commun.* **2**, 1–6 (2011).
- Yang, H., Trouillon, R., Huszka, G. & Gijs, M. A. M. Super-resolution imaging of a dielectric microsphere is governed by the waist of its photonic nanojet. *Nano Lett.* **16**, 4862–4870 (2016).
- Gérard, D. et al. Strong electromagnetic confinement near dielectric microspheres to enhance single-molecule fluorescence. *Opt. Express* **16**, 15297 (2008).
- Xing, C. et al. Flexible microsphere-embedded film for microsphere-enhanced Raman spectroscopy. *ACS Appl Mater. Interfaces* **9**, 32896–32906 (2017).
- Gašparić, V., Ristić, D., Gebavi, H. & Ivanda, M. Resolution and signal enhancement of Raman mapping by photonic nanojet of a microsphere. *Appl. Surf. Sci.* **545**, (2021).
- Li, X., Chen, Z., Taflove, A. & Backman, V. Optical analysis of nanoparticles via enhanced backscattering facilitated by 3-D photonic nanojets. *Opt. Express* **13**, 526 (2005).
- Li, Y. C. et al. Manipulation and detection of single nanoparticles and biomolecules by a photonic nanojet. *Light Sci. Appl.* **5**, (2016).
- Li, Y. et al. Trapping and detection of nanoparticles and cells using a parallel photonic nanojet array. *ACS Nano* **10**, 5800–5808 (2016).
- Bonakdar, A. et al. Deep-UV microsphere projection lithography. *Opt. Lett.* **40**, 2537 (2015).
- Jacassi, A. et al. Scanning probe photonic nanojet lithography. *ACS Appl Mater. Interfaces* **9**, 32386–32393 (2017).
- Ristori, A., Felici, M., Pettinari, G., Pattelli, L. & Biccari, F. Photonic jets and single-photon emitters. *Adv. Photonics Res.* **3**, 1–8 (2022).
- Yang, S., Taflove, A. & Backman, V. Experimental confirmation at visible light wavelengths of the backscattering enhancement phenomenon of the photonic nanojet. *Opt. Express* **19**, 7084 (2011).
- Wang, F. et al. Scanning superlens microscopy for non-invasive large field-of-view visible light nanoscale imaging. *Nat. Commun.* **7**, 1–10 (2016).

28. Krivitsky, L. A., Wang, J. J., Wang, Z. & Luk'Yanchuk, B. Locomotion of microspheres for super-resolution imaging. *Sci. Rep.* **3**, 3–7 (2013).
29. Li, Y., Liu, X. & Li, B. Single-cell biomagnifier for optical nanoscopes and nanotweezers. *Light Sci. Appl.* **8**, (2019).
30. Zhang, T. et al. Fabrication of flexible microlens arrays for parallel super-resolution imaging. *Appl. Surf. Sci.* **504**, 144375 (2020).
31. Shen, K., Lu, H., Baig, S. & Wang, M. R. Improving lateral resolution and image quality of optical coherence tomography by the multi-frame superresolution technique for 3D tissue imaging. *Biomed. Opt. Express* **8**, 4887 (2017).
32. Klini, A. et al. Reproducible optical fiber tips for photon scanning tunneling microscopy with very small (<5°) cone angle. *J. Lightwave Technol.* **16**, 1220–1227 (1998).
33. Kaur, J., Vairagi, K., Minz, R. A., Enoch, S. & Mondal, S. K. Encaved optical fiber nano-probe exciting whispering gallery mode resonance with focused far off-axis beam. *Opt. Express* **31**, 27203 (2023).
34. Mondal, S. K., Pal, S. S. & Kapur, P. Optical fiber nano-tip and 3D bottle beam as non-plasmonic optical tweezers. *Opt. Express* **20**, 16180 (2012).
35. Decombe, J. B., Mondal, S. K., Kumbhakar, D., Pal, S. S. & Fick, J. Single and multiple microparticle trapping using non-gaussian beams from optical fiber nanoantennas. *IEEE J. Selected Top. Quant. Electron.* **21**, (2015).
36. Ward, J. M. et al. Excitation of whispering gallery modes with a “point-and-play,” fiber-based, optical nano-antenna. *Opt. Lett.* **44**, 3386–3389 (2019).
37. Mondal, S. K., Mitra, A., Singh, N., Shi, F. & Kapur, P. Ultrafine fiber tip etched in hydrophobic polymer coated tube for near-field scanning plasmonic probe. *IEEE Photonics Technol. Lett.* **23**, 1382–1384 (2011).
38. Schindelin, J. et al. Fiji: An open-source platform for biological-image analysis. *Nat. Methods* **9**, 676–682 (2012).
39. Gupta, P., Vairagi, K. & Mondal, S. K. All-fiber negative axicon probe with a Bessel beam for cellular-level low coherence phase microscopy and refractive index measurement. *Opt. Lett.* **47**, 497 (2022).
40. Joo, C., Akkin, T., Cense, B., Park, B. H. & de Boer, J. F. Spectral-domain optical coherence phase microscopy for quantitative phase-contrast imaging. *Opt. Lett.* **30**, 2131 (2005).
41. Valli, J. & Sanderson, J. Super-resolution fluorescence microscopy methods for assessing mouse biology. *Curr. Protoc.* **1**, (2021).
42. Dubois, A., Vabre, L., Boccara, A. C. & Beaufrepaire, E. High-resolution full-field optical coherence tomography with a Linnik microscope. *Appl. Opt.* **41**, 805–812 (2002).
43. Scholler, J. et al. Probing dynamic processes in the eye at multiple spatial and temporal scales with multimodal full field OCT. *Biomed. Opt. Express* **10**, 731 (2019).
44. Leitgeb, R. A. En face optical coherence tomography: a technology review. *Biomed. Opt. Exp.* **10**, 2177 (2019).
45. Tsai, C. Y. et al. Submicron spatial resolution optical coherence tomography for visualising the 3D structures of cells cultivated in complex culture systems. *Sci. Rep.* **11**, 1–12 (2021).
46. Beaufrepaire, E., Boccara, A. C., Lebec, M., Blanchot, L. & Saint-Jalmes, H. Full-field optical coherence microscopy. *Opt. Lett.* **23**, 244 (1998).
47. Grieve, K. et al. Ocular tissue imaging using ultrahigh-resolution, full-field optical coherence tomography. *Invest. Ophthalmol. Vis. Sci.* **45**, 4126–4131 (2004).
48. Yue, L. et al. Photonic hook: a new curved light beam. *Opt. Lett.* **43**, 771 (2018).

## Acknowledgements

We acknowledge Prof. Ananth Venkatesan, IISER Mohali for providing FESEM imaging facility. We acknowledge Dr. Vivek Bagchi, INST Mohali for providing silver nanoparticles. We also acknowledge Dr Umesh K Tiwari, CSIR-CSIO for providing computational resources. Pooja Gupta would like to acknowledge the Council of Scientific & Industrial Research (CSIR), New Delhi, India, for Research Associate fellowship. Kaushal Vairagi would like to thank the CSIR FIRST Scheme and CSIR-Research Associate Fellowship 31/0031(19170)/2024-EMR-I for providing financial assistance.

## Author contributions

K.V.: Design and development of experimental setups, Photonic nanojet characterisation, OCT en face imaging, manuscript writing. J.K.: Preparing nanoprobe and Photonic nanojet head, simulation, and manuscript editing. P.G.: Phase microscopy and manuscript editing. S.E.: Participation in discussion and editing the manuscript. S.K.M.: Conceptualizing and formulation of the problem, mentoring the group during entire experimentations and its day-to-day progress, writing and editing the manuscript.

## Competing interests

The authors declare no competing interests.

## Additional information

**Supplementary information** The online version contains supplementary material available at <https://doi.org/10.1038/s42005-025-02007-2>.

**Correspondence** and requests for materials should be addressed to Samir K. Mondal.

**Peer review information** *Communications Physics* thanks the anonymous reviewers for their contribution to the peer review of this work. [A peer review file is available].

**Reprints and permissions information** is available at <http://www.nature.com/reprints>

**Publisher's note** Springer Nature remains neutral with regard to jurisdictional claims in published maps and institutional affiliations.

**Open Access** This article is licensed under a Creative Commons Attribution-NonCommercial-NoDerivatives 4.0 International License, which permits any non-commercial use, sharing, distribution and reproduction in any medium or format, as long as you give appropriate credit to the original author(s) and the source, provide a link to the Creative Commons licence, and indicate if you modified the licensed material. You do not have permission under this licence to share adapted material derived from this article or parts of it. The images or other third party material in this article are included in the article's Creative Commons licence, unless indicated otherwise in a credit line to the material. If material is not included in the article's Creative Commons licence and your intended use is not permitted by statutory regulation or exceeds the permitted use, you will need to obtain permission directly from the copyright holder. To view a copy of this licence, visit <http://creativecommons.org/licenses/by-nc-nd/4.0/>.

© The Author(s) 2025